

## Crystal habits of $\text{LiMn}_2\text{O}_4$ and their influence on the electrochemical performance

K. Ragavendran<sup>a,b</sup>, H.L. Chou<sup>b</sup>, L. Lu<sup>a,\*</sup>, Man On Lai<sup>a</sup>, B.J. Hwang<sup>b</sup>, R. Ravi Kumar<sup>c</sup>, S. Gopukumar<sup>c</sup>, Bosco Emmanuel<sup>c</sup>, D. Vasudevan<sup>c</sup>, D. Sherwood<sup>c</sup>

<sup>a</sup> Materials Laboratory, Department of Mechanical Engineering, National University of Singapore, Singapore 117576, Singapore

<sup>b</sup> Nano Electrochemistry Laboratory, National Taiwan University of Science and Technology, Taipei, Taiwan

<sup>c</sup> Central Electrochemical Research Institute, Karaikudi 630 006, Tamilnadu, India

### ARTICLE INFO

#### Article history:

Received 8 December 2010

Received in revised form 26 May 2011

Accepted 11 July 2011

Available online 27 July 2011

#### Keywords:

Lithium manganate

Crystal habits

Crystal shape algorithm

Density functional theory

Lithium batteries

### ABSTRACT

Crystal habits of  $\text{LiMn}_2\text{O}_4$  prepared through a sol–gel method using different starting materials (metal acetates and metal nitrates) are studied using a crystal shape algorithm. Density functional theory (DFT) as implemented in VASP is employed to study the thermodynamic stabilities and the electronic structure of the different *hkl* planes of  $\text{LiMn}_2\text{O}_4$ , as identified by the crystal shape algorithm. The crystal habit of lithium manganate prepared through the metal acetate route,  $\text{LiMn}_2\text{O}_4$  (A), seems to possess a higher thermodynamic stability compared to the metal nitrate route viz.  $\text{LiMn}_2\text{O}_4$  (N). Electrochemical cycling measurements show that the capacity retention in  $\text{LiMn}_2\text{O}_4$  (A) is better than  $\text{LiMn}_2\text{O}_4$  (N) at low (C/10) as well as at higher (5C) rates.

© 2011 Elsevier B.V. All rights reserved.

### 1. Introduction

The electrochemical performance of a cathode material in a Li-battery depends upon several factors among which (a) crystallographic structure, (b) electronic structure, (c) structure of the solid–electrolyte interface and (d) morphology are the most important.

Size and shape are the two essential attributes that determine the morphology and hence the morphology dependent functionality of polycrystalline materials. Size as measured from the full width at half maximum (FWHM) of an XRD peak (i.e., *hkl*) gives the thickness of the crystallite in one particular direction; however only the shape of a material can provide complete 3-D information on its physico-chemical properties. Studies on material's shapes have recently attracted a lot of interest among the scientists since the report by Ertl, recognized with the award of 2007 Nobel Prize in Chemistry, that the catalytic activity of different planes of Fe differs by several orders of magnitude [1]. In the context of cathode materials for lithium battery applications, crystal habit (shape) which manifests as the morphology of the material is one of the important factors that determine the electrochemical performance.

A change in the morphology and hence the electrochemical performance of the cathode material can be achieved by changing the

method of preparation. The influence of morphology of electroactive materials as determined by SEM/TEM on the electrochemical performance is available in the literature [2–4]. However, quantitative information correlating the crystal shape of the cathode material to its electrochemical performance is not available as yet. This manuscript is our preliminary effort to quantitatively relate the electrochemical performance of a cathode material, such as  $\text{LiMn}_2\text{O}_4$ , with a spinel type structure and an Fd3m space group [5], prepared using different starting materials, to their crystal habits. Since  $\text{LiMn}_2\text{O}_4$  (A) and  $\text{LiMn}_2\text{O}_4$  (N) differ only in the nature of the starting materials used, it is reasonable to believe that a difference in the electrochemical behavior between these cathodes could arise mostly due to the differences in their morphology.

We use the crystal shape algorithm [6] which simulates the crystal habit of  $\text{LiMn}_2\text{O}_4$  from the  $2\theta$  and the full width at half maximum (FWHM) values for the X-ray reflections arising from the corresponding Miller indices of the material. DFT computations were carried out to compute the thermodynamic stabilities of the predominant *hkl* planes as identified by the crystal shape algorithm.

It is well known in electrochemistry that many physical and electrochemical properties such as electronic work functions, catalytic rates of reactions and adsorption kinetics depend on the surface chemistry/physics. The same holds good with the electrochemistry of lithium batteries which needs the so-called 8a sites accessible to the Li ion coming from the electrolyte. Thus the Li intercalation depends not only on the surface density of 8a sites exposed on a given plane but also on the hindrance offered by the surrounding ions on the plane. Both the density and the

\* Corresponding author. Tel.: +65 65162236; fax: +65 6779 1459.

E-mail address: [luli@nus.edu.sg](mailto:luli@nus.edu.sg) (L. Lu).

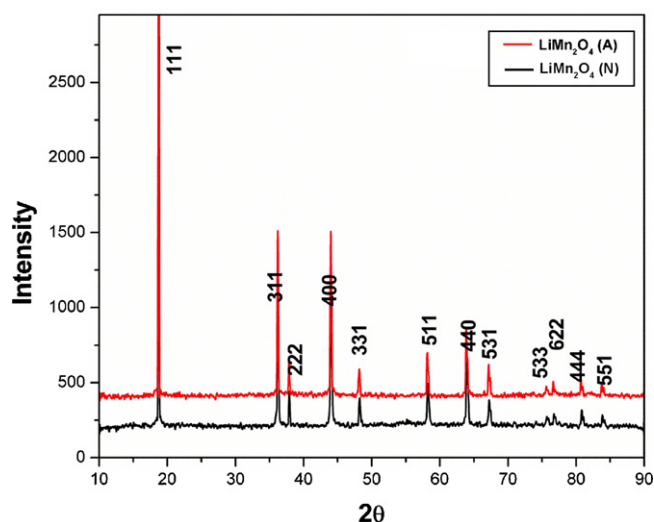


Fig. 1. X-ray diffraction patterns for LiMn<sub>2</sub>O<sub>4</sub> (A) and LiMn<sub>2</sub>O<sub>4</sub> (N).

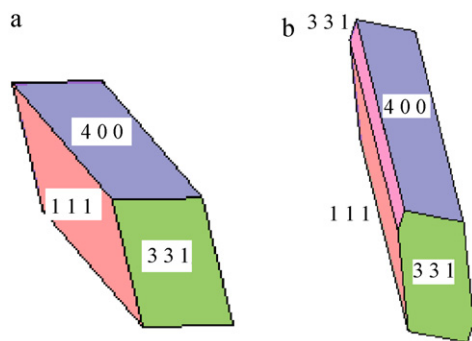


Fig. 2. (a) Crystal habit of LiMn<sub>2</sub>O<sub>4</sub> (A) as predicted by the crystal shape algorithm. (b) Crystal habit of LiMn<sub>2</sub>O<sub>4</sub> (N) as predicted by the crystal shape algorithm.

arrangement of the various ions or vacant sites depend on the Miller plane located on the surfaces. Hence the crystal habit with a given set of Miller planes on the surface and their areas are crucial in determining the electrochemical performance.

In this manuscript we find that the crystal habit of LiMn<sub>2</sub>O<sub>4</sub> (A) is thermodynamically more stable than LiMn<sub>2</sub>O<sub>4</sub> (N). In tune with this observation, electrochemical potential cycling measurements show that capacity fading is lesser in LiMn<sub>2</sub>O<sub>4</sub> (A) compared to LiMn<sub>2</sub>O<sub>4</sub> (N).

## 2. Characterization methods

### 2.1. Experimental part

LiMn<sub>2</sub>O<sub>4</sub> was prepared through a citric acid assisted sol-gel method with metal acetates [designated LiMn<sub>2</sub>O<sub>4</sub> (A)] or metal nitrates [designated LiMn<sub>2</sub>O<sub>4</sub> (N)] as the starting materials. In either case, the corresponding lithium salt, manganese salt and citric acid in the molar ratio of 1:2:3 were dissolved in minimum amount of distilled water and stirred at 80 °C until a gel was formed. LiMn<sub>2</sub>O<sub>4</sub> powder was obtained by calcining the gel at 800 °C for 10 h at a heating/cooling rate of 5 °C min<sup>-1</sup>. X-ray diffraction pattern of the materials were recorded using PANalytical XRD machine with Cu K $\alpha$  radiation. The XRD pattern (Fig. 1) agreed well with the JCPDS data (35-0782) for spinel type LiMn<sub>2</sub>O<sub>4</sub>. Morphology of the cathode materials was recorded with a Hitachi, Model S 3000 H, scanning electron microscope. The composite electrode was made by mixing 80% (weight) LiMn<sub>2</sub>O<sub>4</sub> sample, 10% (weight) carbon black and 10%

Table 1

The  $I_{311}/I_{400}$  ratio and the full width at half maximum (FWHM) of the X-ray reflections from 3 1 1 and 4 0 0 planes for LiMn<sub>2</sub>O<sub>4</sub> (A) and LiMn<sub>2</sub>O<sub>4</sub> (N).

Cathode material	$I_{311}/I_{400}$	FWHM <sub>311</sub>	FWHM <sub>400</sub>
LiMn <sub>2</sub> O <sub>4</sub> (A)	0.88	0.24	0.264
LiMn <sub>2</sub> O <sub>4</sub> (N)	0.93	0.264	0.24

Table 2

Nature and area of the  $hkl$  planes exposed in LiMn<sub>2</sub>O<sub>4</sub> (A) and LiMn<sub>2</sub>O<sub>4</sub> (N). The thermodynamic stabilities of the different  $hkl$  planes (computed using DFT as implemented in VASP) are provided in square brackets. The energetically un-favorable plane is shown in red.

Exposed $hkl$ planes in LiMn <sub>2</sub> O <sub>4</sub> (A) {Area in Å <sup>2</sup> } [surface energy in eV/Å <sup>2</sup> ]	Exposed $hkl$ planes in LiMn <sub>2</sub> O <sub>4</sub> (N) {Area in Å <sup>2</sup> } [surface energy in eV/Å <sup>2</sup> ]
(1 1 1) {205664} [-5.690]	(1 1 1) {244678} [-5.690]
(4 0 0) {177357} [-2.678]	(4 0 0) {197641} [-2.678]
(3 3 1) {158738} [-1.019]	(3 1 1) {72963} [-1.655]
	(3 3 1) {350315} [-1.019]

(weight) poly vinylidene fluoride (binder) in N-methyl pyrrolidone as solvent, followed by stirring the mixture overnight to get homogeneous slurry, which was coated over an aluminum foil and dried for 30 h at 120 °C in vacuum (-76 cm Hg). Swagelok type cells were assembled in a glove box (M-Braun) glove box using two celgard separators, 1 M LiPF<sub>6</sub> dissolved in EC/DEC 50:50 as the electrolyte and Li-foil as the anode. The oxygen and moisture level inside the glove box were maintained at <1 ppm. Electrochemical potential cycling measurements were then made between 3 and 4.6 V, with cycle life tester (Maccor model 4304) at room temperature at C/10 and 5C rates. Complex plane impedance measurements on cycled cells were carried out using Solartron SI 1267 AC impedance analyzer, in the frequency region 1 to 10 mHz.

### 2.2. Computational part

A crystal shape algorithm [6] was used to study the crystal habits and the nature of the exposed  $hkl$  planes in LiMn<sub>2</sub>O<sub>4</sub> (the inputs to the algorithm are the lattice parameter, the miller index ( $h, k, l$ ), the  $2\theta$  value and the full width at half-maximum for each XRD peak). Computations were carried out on a 2.80 GHz Pentium IV processor. The thermodynamic stability and electronic properties of the different  $hkl$  planes of LiMn<sub>2</sub>O<sub>4</sub> were computed using DFT as implemented in VASP. For the DFT computations, the pseudo potential plane wave basis set [7] and the exchange correlation functional based on Ceperley and Alder as parameterized by Perdew and Zunger [8] was adopted. Optimized ultra-soft Vanderbilt pseudo potential for every atom [9] was used in the calculations.

The convergence tests of the total energy with respect to the plane-wave energy cut off and  $k$ -point sampling have been carefully examined and the final series of energies were computed with an energy cutoff of 400 eV, and integration using 10  $k$ -point sampling over the super cell irreducible Brillouin zone, generated by the Monkhorst-Pack scheme [10]. This set of parameters assures

**Table 3**Table showing that *hkl* planes in which Mn atoms are deeply buried are thermodynamically most stable.

<i>hkl</i> plane [surface energy in eV/Å <sup>2</sup> ]	Super cell dimension (Å <sup>3</sup> ) and the formula unit	Distance of the nearest and the farthest Mn from the surface (Å)
(1 1 1) [-5.690]	5.831 × 5.831 × 22.928 Li <sub>2</sub> O <sub>8</sub> Mn <sub>5</sub>	Mn <sub>(nearest)</sub> : 1.19 Mn <sub>(farthest)</sub> : 7.52
(4 0 0) [-2.678]	13.040 × 5.831 × 16.128 Li <sub>3</sub> O <sub>12</sub> Mn <sub>4</sub>	Mn <sub>(nearest)</sub> : 1.493 Mn <sub>(farthest)</sub> : 1.493
(3 1 1) [-1.655]	5.831 × 5.831 × 18.166 Li <sub>2</sub> O <sub>8</sub> Mn <sub>4</sub>	Mn <sub>(nearest)</sub> : 0.7967 Mn <sub>(farthest)</sub> : 1.046

a total energy convergence of 1 meV per atom. A slab of length 14 Å was constructed over the LiMn<sub>2</sub>O<sub>4</sub> crystal cleaved along the *hkl* plane of interest. Geometry optimization was then carried out to ascertain the surface energy of the *hkl* plane. The distance between the Mn atoms from the surface of a given *hkl* plane was also computed. All the computations were performed using the HP Cluster Platform 4000 facility from National Center for High-Performance Computing (NCHC, Taiwan).

### 3. Results and discussion

#### 3.1. XRD pattern of LiMn<sub>2</sub>O<sub>4</sub> (A) and LiMn<sub>2</sub>O<sub>4</sub> (N)

The XRD pattern of LiMn<sub>2</sub>O<sub>4</sub> (A) and LiMn<sub>2</sub>O<sub>4</sub> (N), shown in Fig. 1, indicates that the synthesized materials agree with the JCPDS for spinel type LiMn<sub>2</sub>O<sub>4</sub> and hence are phase pure. From the XRD

patterns we see that the reflections as given by the  $2\theta$  values are practically the same for both the samples and hence possess similar crystal structures. In the present manuscript we do not go for a detailed study on the internal crystal structure, however, crystal structure data such as the space group and the crystal class very much enters the crystal shape algorithm as detailed in the original paper [6].

Slight differences in the intensity ratios [ $I_{311}/I_{400}$ ] between the two compounds can be noticed in (Table 1). The differences in the intensity ratios reflect possible site exchange between Li and Mn atoms without affecting the crystal structure. It is known from the literature [11] that the so called confused degree ‘ $\gamma$ ’ which indicates the extent of site exchange between Li and Mn atoms decreases with a decrease in the [ $I_{311}/I_{400}$ ] intensity ratio. Furthermore, it is reported that the electrochemical performance increases with a decrease in the ‘ $\gamma$ ’.

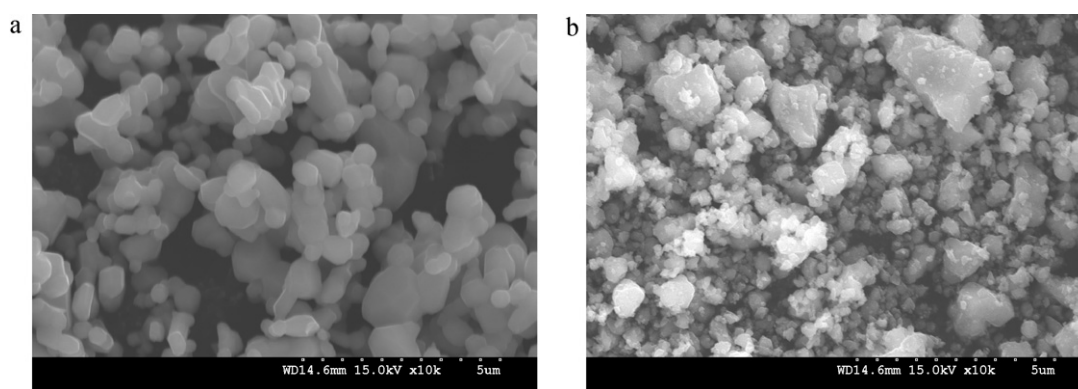


**Fig. 3.** (a) SEM image of LiMn<sub>2</sub>O<sub>4</sub> (A) at a magnification of 10 K. (b) SEM image of LiMn<sub>2</sub>O<sub>4</sub> (N) at a magnification of 10 K.

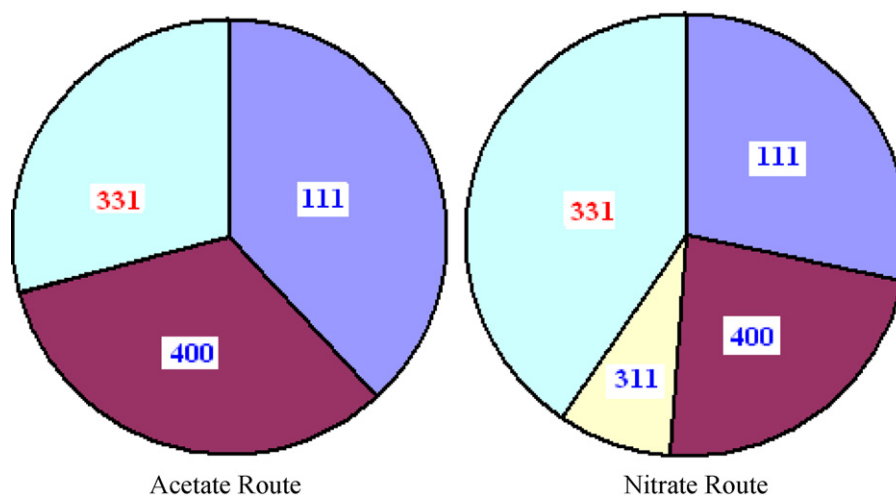


**Fig. 4.** Pie chart showing the extent of exposure of the different *hkl* planes in LiMn<sub>2</sub>O<sub>4</sub> prepared through the acetate route and through the nitrate route. The thermodynamically least stable planes are marked in red. (For interpretation of the references to color in this figure legend, the reader is referred to the web version of the article.)

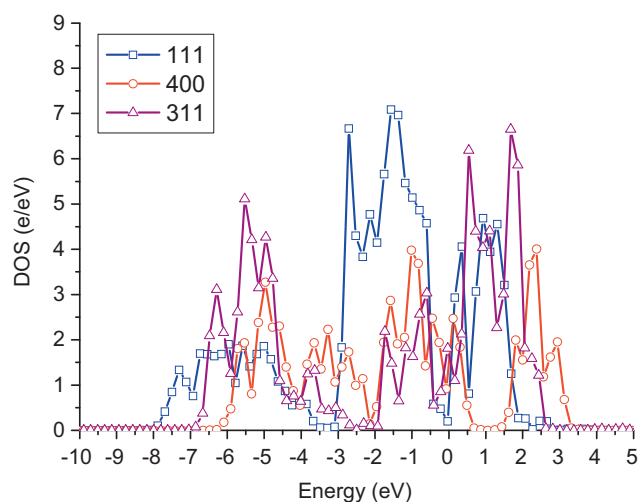


Fig. 5. Mn-3d DOS for the various  $hkl$  planes in  $\text{LiMn}_2\text{O}_4$ .

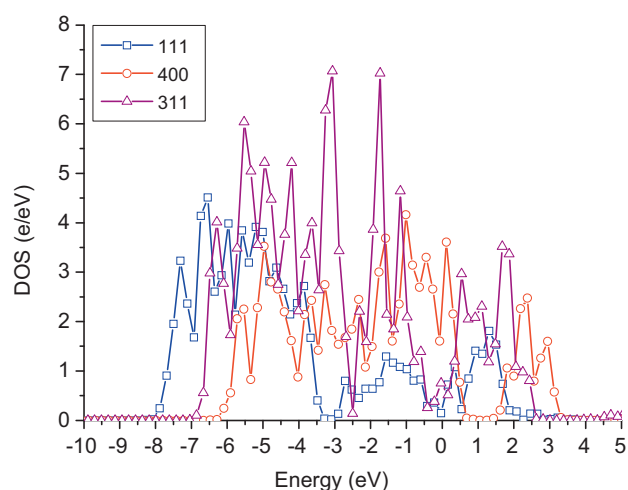


Fig. 6. O-2p DOS for the various  $hkl$  planes in  $\text{LiMn}_2\text{O}_4$ .

From Table 1, it can be seen that among  $\text{LiMn}_2\text{O}_4$  (A) and  $\text{LiMn}_2\text{O}_4$  (N), the former acquires a lower value of  $[I_{311}/I_{400}]$  ratio, indicating at a first glance that the cathode material prepared using metal acetates should possess better electrochemical properties compared to that prepared using metal nitrates.

### 3.2. The crystal shape algorithm and the external crystal shape

The mathematical basis of the algorithm was dealt with in detail in the original paper by Emmanuel and colleagues [6]. The crystal shape algorithm functions on the basis of Scherrer formula and on the fact that the XRD peak of a material arises from a set of parallel and well defined crystal planes having an orientation in space as defined by the Miller indices. Thus, the algorithm takes in the FWHM and  $2\theta$  values of the XRD peaks arising from at least 3 different Miller planes of the given material as the inputs and simulates the crystal habit (shape) by constructing a mathematical envelope from the real points of intersection and discarding the virtual points of intersection. The algorithm thus simulates the crystal habit of the material, assigns the exposed  $hkl$  plane with a unique miller index (which is not straight forward with SEM/TEM) and also ascertains the area of the exposed planes.

The crystal shape algorithm has already demonstrated its success in simulating the crystal habits of materials such as Ge, ZnO,

**Table 4**  
Area of Mn-3d DOS and O-2p DOS below the Fermi level for the different  $hkl$  planes of  $\text{LiMn}_2\text{O}_4$ .

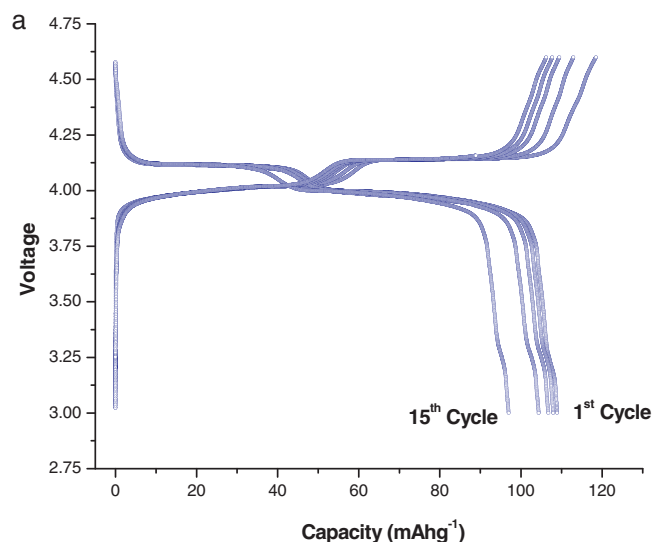
$hkl$ plane	Mn-3d DOS <sup>a</sup>	O-2p DOS <sup>b</sup>	Difference in DOS <sup>c</sup>	Surface energy <sup>d</sup>
(1 1 1)	18.05	14.370	4.320	-5.690
(4 0 0)	10.89	13.696	2.806	-2.678
(3 1 1)	13.33	21.374	8.044	-1.655

<sup>a</sup> Area of Mn-3d DOS below the Fermi level.

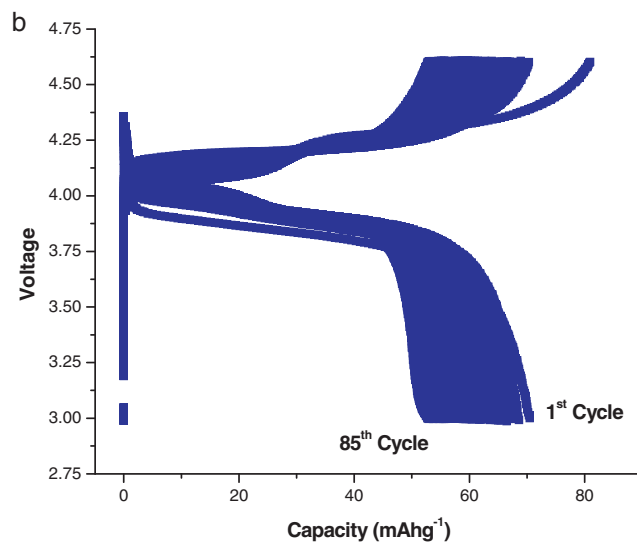
<sup>b</sup> Area of O-2p DOS below the Fermi level.

<sup>c</sup> Difference in the area of Mn-3d DOS and O-2p DOS below the Fermi level.

<sup>d</sup> Surface energy of the  $hkl$  plane in units of  $\text{eV}/\text{\AA}^2$ .



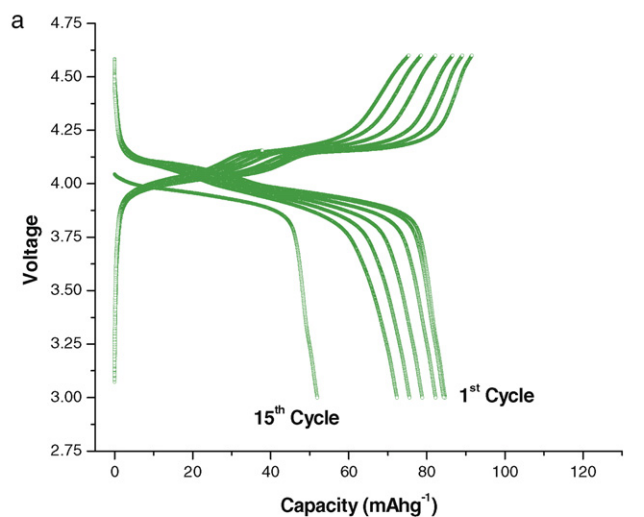
Charge and discharge curves of  $\text{LiMn}_2\text{O}_4$ (A) cycled at C/10 rate



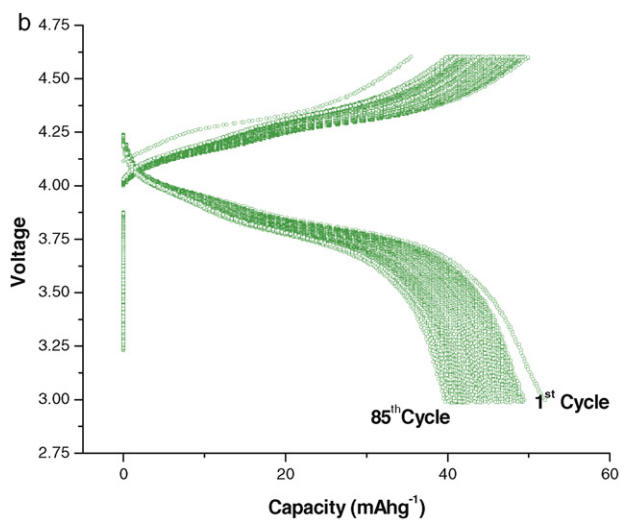
Charge and discharge curves of  $\text{LiMn}_2\text{O}_4$ (A) cycled at 5C rate

Fig. 7. (a) Discharge curve of  $\text{LiMn}_2\text{O}_4$  (A) at C/10 rate. (b) Discharge curve of  $\text{LiMn}_2\text{O}_4$  (A) at 5C rate.

$\text{In}_2\text{O}_3$  and  $\text{MnFe}_2\text{O}_4$ , from their XRD data [6]. The algorithm has several merits as indicated here [6]. Unlike the state of the art computational methods [12–15] that predict the crystal shapes, the algorithm takes inputs from experiment (XRD pattern) and generates the average crystal shape as actually realized in experi-



Charge and discharge curves of  $\text{LiMn}_2\text{O}_4$  (N) cycled at C/10 rate



Charge and discharge curves of  $\text{LiMn}_2\text{O}_4$  (A) cycled at 5C rate

**Fig. 8.** (a) Discharge curve of  $\text{LiMn}_2\text{O}_4$  (N) at C/10 rate. (b) Discharge curve of  $\text{LiMn}_2\text{O}_4$  (N) at 5C rate.

ments. Furthermore, unlike electron microscopy techniques (SEM and TEM), the algorithm provides a complete 3D picture of the crystal in addition to assigning unique miller indices to the predominant  $hkl$  planes.

Fig. 2a and b shows the crystal shapes of  $\text{LiMn}_2\text{O}_4$  (A) and  $\text{LiMn}_2\text{O}_4$  (N) as generated by the crystal shape algorithm. Clear differences in the crystal shape of these two materials can be seen. SEM images of these materials are shown in Fig. 3a and b for comparison. From the SEM pictures, it can be seen that the acetate route has yielded  $\text{LiMn}_2\text{O}_4$  with a better shape and size distribution as compared to the material prepared through the nitrate route. This could be attributed to the fact that when metal acetates, which are salts of weak acid and weak base, are dissolved in water, they undergo salt hydrolysis which maintains a neutral pH of the solution ( $\sim 7$ ), while the metal nitrates are salts of strong acid and weak base and their salt hydrolysis produces an acidic medium with  $\text{pH} < 7$ . Thus, it is the neutral pH provided by the acetate route that encourages the formation of well defined shapes.

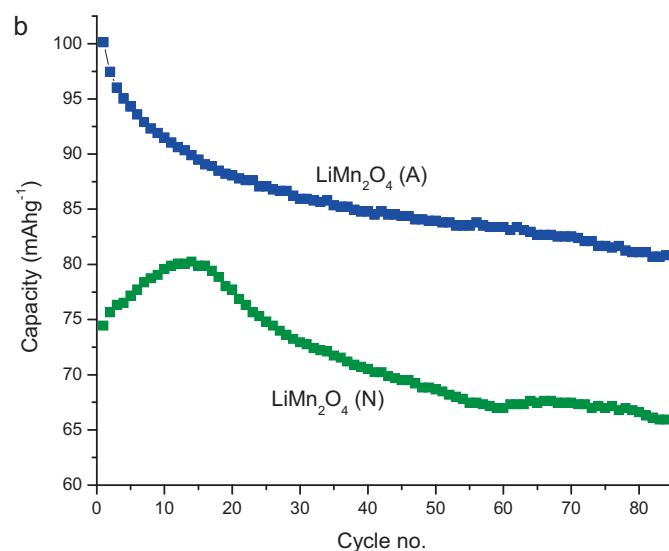
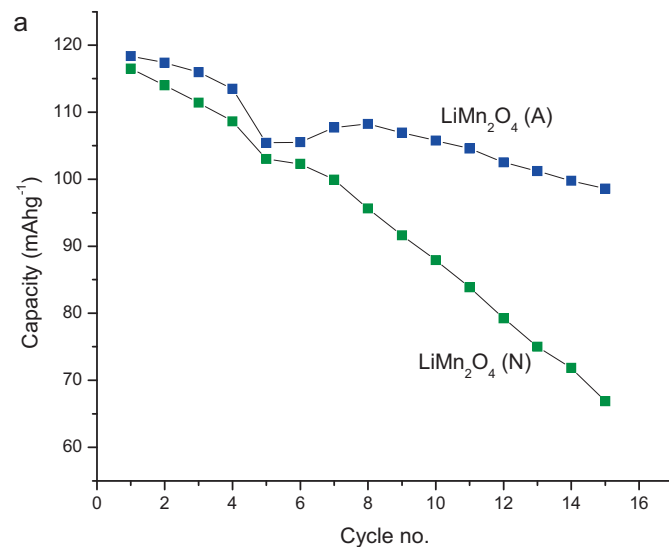


**Fig. 9.** (a) Cyclability curves for the discharge of  $\text{LiMn}_2\text{O}_4$  (A) and  $\text{LiMn}_2\text{O}_4$  (N) at C/10 rate. (b) Cyclability curve for the discharge of  $\text{LiMn}_2\text{O}_4$  (A) and  $\text{LiMn}_2\text{O}_4$  (N) at 5C rate.

It can also be seen that there are some significant differences between the crystal shapes as generated by the crystal shape algorithm and the shape as seen using SEM. We have already discussed in our earlier paper [16] that there need not be a one to one correspondence between the morphology and the underlying crystal habits.

Furthermore, while the shape/habit is a property which depends upon the individual crystallite, the morphology is a result of an agglomeration of a large number of crystallites. Therefore there need not be a one to one correspondence between the morphology (as seen using SEM or TEM) and the underlying crystal habits.

Table 2 shows that the predominant planes in  $\text{LiMn}_2\text{O}_4$  (A) follow the order  $(111) > (400) > (331)$  while that for  $\text{LiMn}_2\text{O}_4$  (N) follow the order  $(331) \gg (111) > (400) > (311)$ . By predominant planes, we mean those  $hkl$  directions along which the rate of crystal growth is minimum, compared to the other  $hkl$  directions, and hence are exposed in accordance with Wulff's rule. Thus the  $(111)$

plane, which will be shown in our forth coming discussions to be the thermodynamically most stable plane, is more predominant in  $\text{LiMn}_2\text{O}_4$  (A) compared to that in  $\text{LiMn}_2\text{O}_4$  (N). The nature and extent of exposure of different  $hkl$  planes in  $\text{LiMn}_2\text{O}_4$  (N) and  $\text{LiMn}_2\text{O}_4$  (A), as generated by the crystal shape algorithm, and furnished in Table 2, are pictorially represented in the pie chart (Fig. 4).

### 3.3. Thermodynamic stability of the $hkl$ planes

Following the quantitative information provided by the crystal shape algorithm on the predominant  $hkl$  planes in  $\text{LiMn}_2\text{O}_4$ , the atomic arrangement on the predominant crystal planes will determine the shape/morphology dependent electrochemical performance of the cathode material. In our earlier paper [16], we only attempted a qualitative study on the atomic arrangement of  $\text{LiMn}_2\text{O}_4$  planes cleaved along the different  $hkl$  directions and classified the planes into (a) favorable planes viz. (111), (311), (400) and (b) un-favorable planes viz. (331), (511), (551) based on whether the Mn atom is lying on the plane or is deeply buried. The DFT computations on the surface energies of the  $hkl$  planes of  $\text{LiMn}_2\text{O}_4$  (Table 3) show that our earlier classification [16] is correct and also that the favorable planes of  $\text{LiMn}_2\text{O}_4$  are thermodynamically more stable than the un-favorable planes. Thus, the thermodynamic stability of the  $hkl$  planes in  $\text{LiMn}_2\text{O}_4$  follows the order (111) > (400) > (311) > (511) > (331) > (551), and the extent to which the Mn atom is buried deep inside a given  $hkl$  plane of  $\text{LiMn}_2\text{O}_4$  also follows the same order.

It is pertinent to note at this point that closeness of an atom to the surface is indeed important for electrochemistry where the seat of reactions is in a thin electrical double layer at the particle/electrolyte interface. The ions close to this interface feel the electrical field which drives all electrochemical reactions be it Li intercalation or other redox or charge-transfer reactions. Besides, the closeness of an atom or ion to this electrochemical interface further enables even purely chemical interactions with the species present in the adjoining electrolyte.

From Tables 2 and 3 it can be seen that the predominant  $hkl$  planes in  $\text{LiMn}_2\text{O}_4$  (A) are those that possess higher thermodynamic stability. This is not the case with  $\text{LiMn}_2\text{O}_4$  (N), which clearly indicates that the crystal habit of  $\text{LiMn}_2\text{O}_4$  (A) is more stable than the crystal habit of  $\text{LiMn}_2\text{O}_4$  (N).

### 3.4. Electronic structure computations

Figs. 5 and 6 present the local density of states (DOS) for the Mn-3d and O-2p levels in the various  $hkl$  planes of  $\text{LiMn}_2\text{O}_4$  with an Fd3m space group. The integrated area of DOS below the Fermi level ( $E_F$ ), which gives a direct measure of the charge state of the atom, is given in Table 4. It can be seen that the density of states (DOS) of the Mn-3d levels below the Fermi level ( $E_F$ ) follows the trend (111) > (311) > (400). Table 4 also shows that the O-2p DOS below the  $E_F$  is much higher than that for the corresponding Mn-3d DOS. This observation is consistent with earlier reports that the redox activity is centered on the oxygen rather than the transition metal atom [17].

If the difference between the Mn-3d DOS and the O-2p DOS of a given  $hkl$  plane could be taken as an indication of the polarity of the plane, we can see from Table 4 that the polarity of the planes follows the order (111) < (400) < (311) and that the thermodynamic stability follows the order (111) > (400) > (311) indicating that planes with a lower polarity possess a higher thermodynamic stability, in accordance with a very recent report [18] which points out that polar surfaces are less stable and that interesting polygonal shapes arises from the polarity of the surface facets. Thus, it

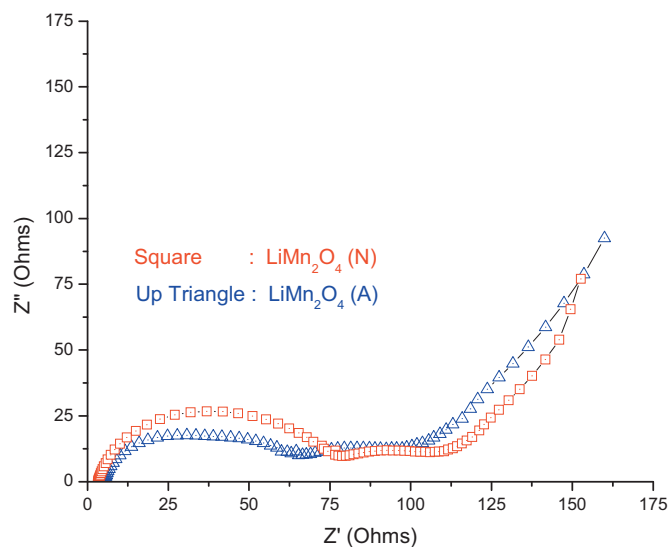


Fig. 10. Complex plane impedance measurements on  $\text{LiMn}_2\text{O}_4$  (A) and  $\text{LiMn}_2\text{O}_4$  (N) at 5C rate.

makes sense if one could argue that shape change in a functional material during the progress of an electrochemical process could be anticipated if the predominant planes in the material are thermodynamically less stable. From these arguments, one could expect that  $\text{LiMn}_2\text{O}_4$  (N) with a crystal habit of lower thermodynamic stability is prone for shape change upon repeated cycling, with the shape change having its own impact on the electrochemical performance.

## 4. Electrochemical potential cycling measurements

The discharge curves of  $\text{LiMn}_2\text{O}_4$  (A) at C/10 and 5C rates are presented respectively in Fig. 7a and b and those for  $\text{LiMn}_2\text{O}_4$  (N) at identical discharge rates are shown in Fig. 8a and b. The cyclability curves for  $\text{LiMn}_2\text{O}_4$  (A) and  $\text{LiMn}_2\text{O}_4$  (N) at C/10 and 5C rates are respectively shown in Fig. 9a and b. It is evident from these figures that  $\text{LiMn}_2\text{O}_4$  (A), with a thermodynamically stable crystal habit, shows better capacity retention and that it also possesses a higher initial capacity compared to  $\text{LiMn}_2\text{O}_4$  (N).

## 5. AC-impedance measurements on $\text{LiMn}_2\text{O}_4$ (A) and $\text{LiMn}_2\text{O}_4$ (N)

The oxide-carbon contact is a very important factor that could decide the electrochemical performance of lithium batteries. However, since the size of the carbon particles are much smaller than the size of the active material particles, the carbon particles almost coat over the active material particles, and hence should lead to an almost identical oxide-carbon contact pattern in the case of both the cathode materials.

In order to address this issue, complex plane AC-impedance measurements on  $\text{LiMn}_2\text{O}_4$  (A) and  $\text{LiMn}_2\text{O}_4$  (N) cells cycled at 5C rates are shown in Fig. 10. It can be seen that the impedance patterns of both  $\text{LiMn}_2\text{O}_4$  (A) and  $\text{LiMn}_2\text{O}_4$  (N) are almost identical, except for a higher angle of depression in the  $\text{LiMn}_2\text{O}_4$  (A) cell. The fact that the charge transfer resistance ( $R_{ct}$ ) and the Warburg parameters ( $W_o$ ) in both the cells are almost identical, shows that the  $\text{LiMn}_2\text{O}_4$  - carbon conducting pathways in  $\text{LiMn}_2\text{O}_4$  (A) is almost similar to  $\text{LiMn}_2\text{O}_4$  (N). The higher angle of depressed semi-circle in  $\text{LiMn}_2\text{O}_4$  (A) could be due to SEI layer which could have its origin from the interaction of the cathode material (with a given

crystal habit) with the electrolyte. Detailed investigations are in progress [19].

## 6. Conclusions

This is the first time that an attempt has been made to quantitatively study the influence of crystal shape of cathode materials, as actually realized in experiments, on Li-battery performance. We used a crystal shape algorithm [6], that can handle both nano and micron sized crystals, to study the crystal habits of  $\text{LiMn}_2\text{O}_4$  prepared through citric acid assisted sol–gel method using metal acetates and metal nitrates as the starting materials.

SEM studies showed that well defined shape distribution could be obtained through the acetate route ( $\text{pH} \sim 7$ ) compared to the nitrate route ( $\text{pH} < 7$ ). In tune with the experimental observations, our simulations predicted that the material prepared through the sol–gel route with metal acetates as the starting materials had acquired a thermodynamically stable crystal habit compared to the material prepared with metal nitrate precursors. Electrochemical cycling measurements show that  $\text{LiMn}_2\text{O}_4$  (A) with a thermodynamically favorable crystal habit shows a better capacity retention, at both lower (C/10) and higher (5C) rates, compared to  $\text{LiMn}_2\text{O}_4$  (N).

AC-impedance measurements on  $\text{LiMn}_2\text{O}_4$  (A) and  $\text{LiMn}_2\text{O}_4$  (N) cells showed almost identical patterns. Quantitative studies on shape of the functional material thus seem to be an important issue in lithium battery research. The approach presented in this paper will be extended in our future research to nano scales where surface effects are more dominant.

## Acknowledgements

The authors thank the National University of Singapore for the funding and the experimental facility needed to carry out the electrochemical measurements. National Center for High-Performance Computing (NCHC, Taiwan) is gratefully acknowledged for the permission to carry out the DFT computations.

## References

- [1] G. Ertl, Catal. Rev. Sci. Eng. 21 (1980) 201.
- [2] H.-L. Zhu, Z.-Y. Chen, S. Ji, V. Linkov, Solid State Ionics 179 (2008) 1788.
- [3] T. Ogihara, H. Aikiyo, N. Ogata, K. Katayama, Y. Azuma, H. Okabe, T. Okawa, Adv. Powder Technol. 13 (2002) 437.
- [4] T. Le Mercier, J. Gaubicher, E. Bermejo, Y. Chabre, M. Quarton, J. Mater. Chem. 9 (1999) 567.
- [5] K. Ragavendran, A. Nakkiran, P. Kalyani, A. Veluchamy, R. Jagannathan, Chem. Phys. Lett. 456 (2008) 110.
- [6] D. Sherwood, B. Emmanuel, Cryst. Growth Des. 6 (2006) 1415.
- [7] G. Kresse, J. Hafner, Phys. Rev. B 49 (1994) 14, 951.
- [8] J.P. Perdew, A. Zunger, Phys. Rev. B 23 (1981) 5048.
- [9] D. Vanderbilt, Phys. Rev. B 41 (1990) 7892.
- [10] H.J. Monkhorst, J.D. Pack, Phys. Rev. B 13 (1976) 5188.
- [11] T.F. Yia, C.L. Hao, C.B. Yue, R.S. Zhu, J. Shu, Synthetic Met. 159 (2009) 1255.
- [12] R.V. Ramanujan, Mater. Sci. Eng. B 32 (1995) 125.
- [13] R. Docherty, G. Clydesdale, K.J. Roberts, P. Bennema, J. Phys. D: Appl. Phys. 24 (1991) 89.
- [14] X.Y. Liu, E.S. Boek, W.J. Briels, P. Bennema, Nature 374 (1995) 342.
- [15] M. Saska, A.S. Myerson, J. Cryst. Growth 61 (1983) 546.
- [16] K. Ragavendran, D. Sherwood, D. Vasudevan, B. Emmanuel, Physica B 404 (2009) 2166.
- [17] G. Ceder, Y.-M. Chiang, D.R. Sadoway, M.K. Aydinol, Y.-I. Jang, B. Huang, Nature 392 (1998) 694.
- [18] B. Koo, R.N. Patel, B.A. Korgel, J. Am. Chem. Soc. 131 (2009) 3134.
- [19] B. Emmanuel, J. Electroanal. Chem. 624 (2008) 14.